# Electronic Supporting Information

# Investigating the role of Cu-oxo species in Cu-nitrates formation over Cu-CHA catalysts

*Chiara Negri,*[a1] *A. Martini,*[a,b] *G. Deplano,*[a] *Kirill A. Lomachenko,*[c] *Ton V. W. Janssens,*[d] *Elisa Borfecchia,*[a] **Gloria Berlier* [a] ** and Silvia Bordiga* [a]

[a] Department of Chemistry and NIS Centre, University of Turin, Via Giuria 7, Turin, 10125 (I)

[b] The Smart Materials Research Institute, Southern Federal University, Sladkova 178/24, 344090 Rostov-on-Don, Russia

[c] European Synchrotron Radiation Facility, 71 Avenue des Martyrs, CS 40220, 38043 Grenoble Cedex 9, France

[d] Umicore Denmark ApS, Kogle Allé 1, 2970 Hørsholm, Denmark

## Table of Contents



[1] Current address: Laboratory of Catalysis and Catalytic Processes, Department of Energy, Politecnico di Milano, Via La Masa 34, 20156, Milano (Italy)

# 1 Infrared spectra at 50 °C on Cu-CHA 0.1_5

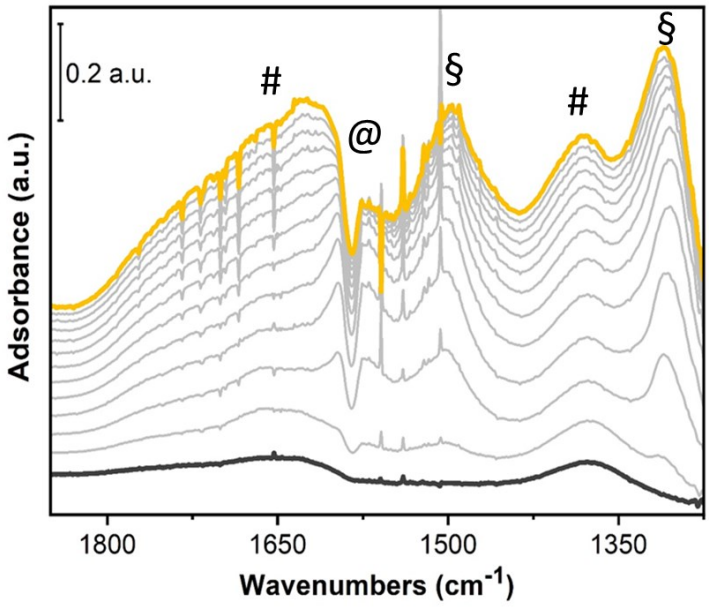


**Figure S1:** In situ FTIR spectra of Cu-CHA 0.1_5 exposed to 1000 ppm NO/10% $O_2$ at 50 °C, after pre-treatment in $O_2$. Spectra are background subtracted using the spectrum measured at the same temperature before NO/$O_2$ dosage, and are reported as a function of time during the interaction with NO/$O_2$ (from black to yellow)

The spectra are dominated by the broad bands due to the formation of $H_2O/H^+$ adducts, as a result of the reaction of NO/$O_2$ with Brønsted sites (around 1650 and 1380 $cm^{-1}$, indicated with #), with the contribution of bands related to monodentate nitrates (§ symbols, around 1500 and 1310 $cm^{-1}$). The formation of a tiny amount of chelating bidentate nitrates could be suggested by the 'hole' around 1585 cm-1 (@ symbol).[1]

# 2 Two-component EXAFS fits for Cu-CHA 0.2_15

## *2.1 Fitting methods*

The Cu-CHA 0.2_15 catalyst, in line with its compositional characteristics, is confirmed to contain a mixture of two Cu-species by means of LCF analysis. These are best described by the $Z[Cu^{II}OH]$ 8r and $Z_2Cu^{II}$ 6r model pretreatment in $O_2$, and by the $Z[Cu^{II}(NO_3)]$ 8r and $Z_2Cu^{II}$ 6r models after exposure to the NO/$O_2$ mixture at 200 °C. To further deepen the structural analysis for this catalyst, we attempted a series of two-components EXAFS fits on the experimental data obtained for this sample upon pretreatment in $O_2$ and after exposure to the NO/$O_2$ mixture at 200 °C.

The two-components fits were based on LCF analysis for Cu-CHA 0.2_15 as well as EXAFS fitting results obtained for the other two catalysts, thus allowing us to limit the number of fitting variables. In particular, the two-components fits were performed following the same approach adopted for EXAFS analysis of Cu-CHA 0.6_29 and Cu-CHA 0.1_5. However, two sets of scattering paths were generated by FEFF, starting from the two structural models envisaged to contribute to the mixture and individually parametrized as done for single-component fits. In addition, two weights parameters $w_i$ were used to describe the fractions of the two Cu-species, by constraining the sum of the two weights to one ($w_2 = 1-w_1$).

Common $S_0^2$ (set to 0.95 in all cases) and ΔE (guessed) parameters were employed for both sets of paths. For all the included SS and MS contributions, Debye-Waller factors were set to the best fit values obtained in the related single-component fits, while the structural parameters ($R_i$ and $\alpha_{fw}$) were optimized, aiming to check for small rearrangements in the local structure of the Cu-species separately identified in the other, purer, Cu-CHA catalysts.

Importantly, in the presence of Cu-$Cu_{ef}$ scattering contribution (identified also for Cu-CHA 0.2_15 by EXAFS-WT analysis) with sample- and condition-dependent coordination number $N_{Cu\_ef}$, it is impossible to obtain a reliable fit by simultaneously optimizing $N_{Cu\_ef}$ and $w_i$. Thus, we adopted the following three-step refinement approach:

- 1st refinement step: fit run with $w_{1,2}$ set based on LCF (k-space) results and $N_{Cu\_ef}$ guessed;
- 2nd refinement step: fit run $N_{Cu\_ef}$ set to best fit values from 1st refinement step and $w_{1,2}$ guessed;
- 3rd refinement step (final): fit run with $w_{1,2}$ set to best fit values from 2nd refinement step and $N_{Cu\_ef}$ guessed.

## *2.2 Fitting results*

**Table S1:** Results of the two-component fit (3rd and final refinement step) performed on the $k^2$-weighted FT-EXAFS spectrum of Cu-CHA 0.2_15 (transformed in the 2.4-12.0 $Å^{-1}$ k-range) pretreated in $O_2$ at 400 °C and measured after cooling down to 200 °C in $O_2$. Parameter values set in the fit are underlined. For comparison, the table also reports the results from single-component fits performed on Cu-CHA 0.6_29 (using the Z[$Cu^{II}$OH] 8r) and on Cu-CHA 0.1_5 (using the $Z_2Cu^{II}$ 6r model) under the same conditions, already presented in the main text.

| | ***EXAFS parameters*** | ***Best-fit values Cu-CHA 0.2_15 2-comp.*** | ***Best-fit values Cu-CHA 0.6_29 Z[$Cu^{II}$OH] 8r*** | ***Best-fit values Cu-CHA 0.1_5 $Z_2Cu^{II}$ 6r*** |
|---|---|---|---|---|
| | **N°$_{par}$/N°$_{ind}$** | 10/18 | 10/18 | 9/18 |
| | **$R_{factor}$** | 0.00435 | 0.0117 | 0.0065 |
| | **$S_0^2$** | <u>0.95</u> | <u>0.95</u> | <u>0.95</u> |
| | **ΔE (eV)** | -2.7 ± 0.7 | -2 ± 1 | -3.8 ± 0.8 |
| ***Z[$Cu^{II}$OH 8r*** | ***$w_1$*** | <u>0.57 ± 0.09</u> (0.66)[a] | <u>1</u> | <u>0</u> |
| | **$R_{O\ ef}$ (Å)** | 1.88 ± 0.06 | 1.83 ± 0.02 | – |
| | **<$R_{O\ fw}$> (Å)** | 1.93 ± 0.06 | 1.951 ± 0.01 | – |
| | **<$R_{T\ fw}$> (Å)** | 2.71 ± 0.03 | 2.70 ± 0.02 | – |
| | **$\alpha_{fw}$** | - 0.05 ± 0.01 | - 0.02 ± 0.01 | – |
| | **$\sigma^2_{O\ fw}$ ($Å^2$)** | <u>0.003 ± 0.002</u> | 0.003 ± 0.002 | – |
| | **$\sigma^2_{T\ fw}$ ($Å^2$)** | <u>0.009 ± 0.002</u> | 0.009 ± 0.002 | – |
| | **$ss_{fw}$ ($Å^2$)** | <u>0.021 ± 0.008</u> | 0.021 ± 0.008 | – |
| ***$Z_2Cu^{II}$ 6r*** | ***$w_2$*** | <u>0.43 ± 0.09</u> (0.34)[a] | <u>0</u> | <u>1</u> |
| | **<$R_{O\ fw}$> (Å)** | 1.97 ± 0.03 | – | 1.959 ± 0.006 |
| | **<$R_{T\ fw}$> (Å)** | 2.76 ± 0.02 | – | 2.799 ± 0.009 |
| | **$\alpha_{fw}$** | 0.009 ± 0.009 | – | - 0.003 ± 0.005 |
| | **$\sigma^2_{O\ fw}$ ($Å^2$)** | <u>0.004 ± 0.001</u> | – | 0.004 ± 0.001 |
| | **$\sigma^2_{T\ fw}$ ($Å^2$)** | <u>0.008 ± 0.001</u> | – | 0.008 ± 0.001 |
| | **$ss_{fw}$ ($Å^2$)** | <u>0.012 ± 0.002</u> | – | 0.012 ± 0.002 |
| ***Cu-Cu*** | **$R_{Cu\ ef}$ (Å)** | 3.39 ± 0.02 | 3.36 ± 0.05 | 3.41 ± 0.02 |
| | **$\sigma^2_{Cu\ ef}$ ($Å^2$)** | <u>0.01</u> | <u>0.01</u> | <u>0.01</u> |
| | **$N_{Cu\ ef}$** | 0.8 ± 0.2 | 0.4 ± 0.3 | 1.2 ± 0.4 |

[a] Errors on optimized fractions of Cu-species are obtained from the 2nd refinement step; fractions obtained from LCF analysis in k-space used as initial set values in the 1st refinement step are also reported in parentheses.

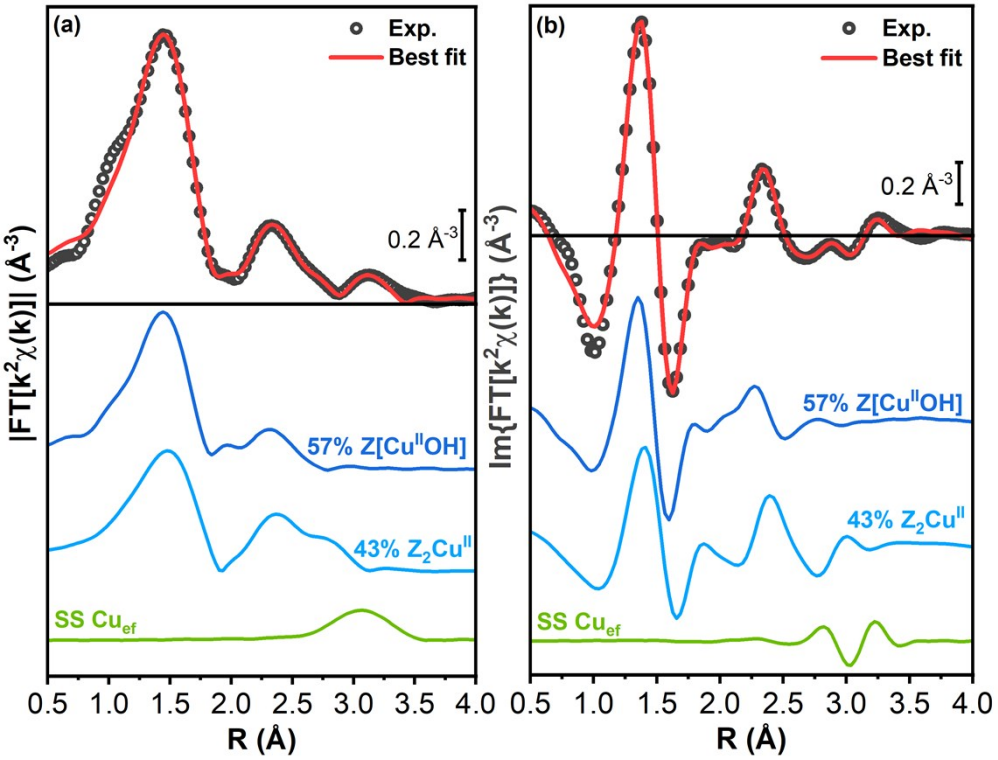


**Figure S2:** Phase-uncorrected (a) modulus and (b) imaginary part of the experimental and two-component best fit FT-EXAFS spectrum for CHA 0.2_15 pretreated in $O_2$ (results from 3rd and final refinement step). The experimental data are shown as black open circles and the best fits with red solid lines. The scaled contributions stemming from each component ($Z[Cu^{II}OH]$ 8r and $Z_2Cu^{II}$ 6r models) are reported together with the optimized Cu-$Cu_{ef}$ SS path as coloured solid lines, vertically translated for sake of clarity.

**Table S2:** Results of the two-component fit (3rd and final refinement step) performed on the $k^2$-weighted FT-EXAFS spectrum of Cu-CHA 0.2_15 (transformed in the 2.4-12.0 $Å^{-1}$ k-range) after exposure to the $NO/O_2$ mixture at 200 °C. Parameter values set in the fit are underlined. For comparison, the table also reports the results from single-component fits performed on Cu-CHA 0.6_29 (using the $Z[Cu^{II}NO_3$ 8r) and on Cu-CHA 0.1_5 (using the $Z_2Cu^{II}$ 6r model) under the same conditions, already presented in the main text.

| | ***EXAFS parameters*** | ***Best-fit values Cu-CHA 02_15 2-comp.*** | ***Best-fit values Cu-CHA06_29 $Z[Cu^{II}NO_3]$ 8r.*** | ***Best-fit values Cu-CHA01_5 $Z_2Cu^{II}$ 6r*** |
|---|---|---|---|---|
| | **$N°_{par}/N°_{ind}$** | 10/18 | 13/18 | 9/18 |
| | **$R_{factor}$** | 0.0061 | 0.005 | 0.0065 |
| | **$S_0^2$** | 0.95 | 0.95 | 0.95 |
| | **ΔE (eV)** | -3.0 ± 0.8 | -3 ± 1 | -3.8 ± 0.8 |
| ***$Z[Cu^{II}NO_3]$ 8r*** | ***$w_1$*** | 0.68 ± 0.02 (0.66)[a] | 1 | 0 |
| | **$<R_{O\ fw}>$ (Å)** | 1.92 ± 0.04 | 1.87 ± 0.03 | – |
| | **$<R_{O1\ NO3}>$ (Å)** | 1.98 ± 0.01 | 1.97 ± 0.02 | – |
| | **$R_{T\ fw}$ (Å)** | 2.72 ± 0.02 | 2.72 ± 0.01 | – |
| | **$\alpha_{fw}$** | - 0.03 ± 0.01 | - 0.04 ± 0.01 | – |
| | **$\sigma^2_{O\ fw}$ ($Å^2$)** | 0.005 ± 0.003 | 0.005 ± 0.003 | – |
| | **$\sigma^2_{O1\ NO3}$ ($Å^2$)** | 0.004 ± 0.002 | 0.004 ± 0.002 | – |
| | **$\sigma^2_{T\ fw}$ ($Å^2$)** | 0.006 ± 0.002 | 0.006 ± 0.002 | – |
| | **$\sigma^2_{N/O2\ NO3}$ ($Å^2$)** | 0.015 ± 0.002 | 0.015 ± 0.002 | |
| | **$\sigma^2_{fw}$ ($Å^2$)** | 0.008 ± 0.002 | 0.008 ± 0.002 | |
| | **$\sigma^2_{MS}$** | 0.009 ± 0.003 | 0.009 ± 0.003 | |
| ***$Z_2Cu^{II}$ 6r*** | ***$w_2$*** | 0.32 ± 0.02 (0.34)[a] | 0 | 1 |
| | **$<R_{O\ fw}>$ (Å)** | 1.92 ± 0.05 | – | 1.959 ± 0.006 |
| | **$<R_{T\ fw}>$ (Å)** | 2.80 ± 0.03 | – | 2.799 ± 0.009 |
| | **$\alpha_{fw}$** | 0.03 ± 0.02 | – | - 0.003 ± 0.005 |
| | **$\sigma^2_{O\ fw}$ ($Å^2$)** | 0.004 ± 0.001 | – | 0.004 ± 0.001 |
| | **$\sigma^2_{T\ fw}$ ($Å^2$)** | 0.008 ± 0.001 | – | 0.008 ± 0.001 |
| | **$ss_{fw}$ ($Å^2$)** | 0.012 ± 0.002 | – | 0.012 ± 0.002 |
| ***Cu-Cu*** | **$R_{Cu\ ef}$ (Å)** | 3.39 ± 0.02 | 3.30 ± 0.08 | 3.41 ± 0.02 |
| | **$\sigma^2_{Cu\ ef}$ ($Å^2$)** | 0.01 | 0.01 | 0.01 |
| | **$N_{Cu\ ef}$** | 0.9 ± 0.3 | 0.3 ± 0.3 | 1.2 ± 0.4 |

[a] Errors on optimized fractions of Cu-species are obtained from the 2nd refinement step; fractions obtained from LCF analysis in k-space used as initial set values in the 1st refinement step are also reported in parentheses.

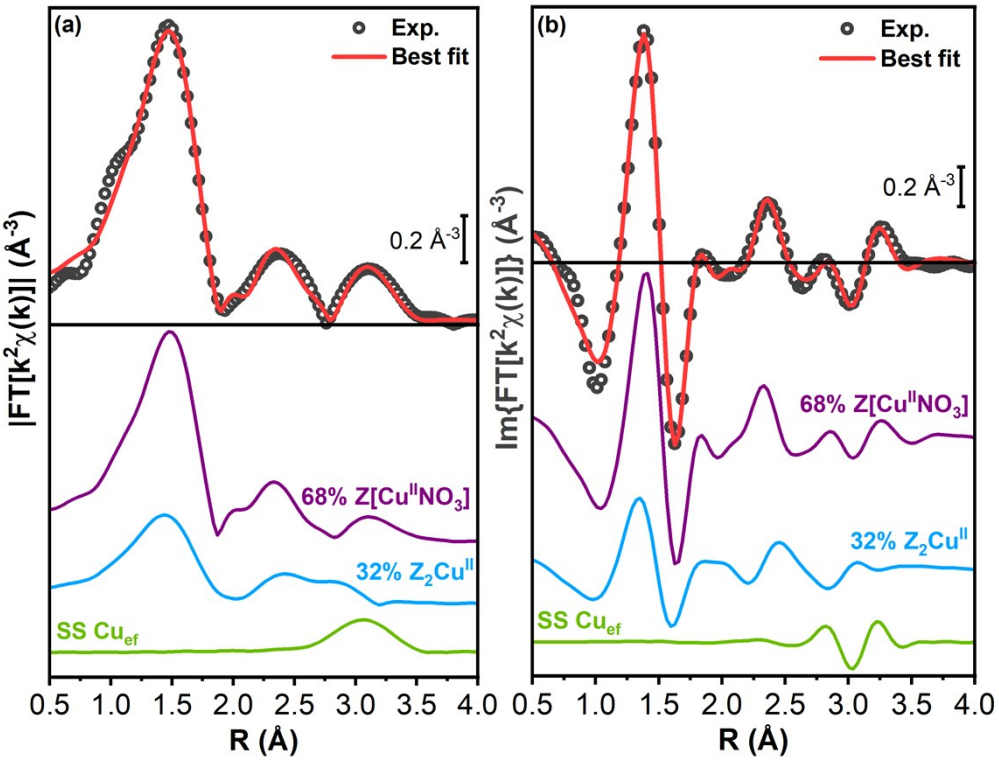


**Figure S3:** Phase-uncorrected (a) modulus and (b) imaginary part of the experimental and two-component best fit FT-EXAFS spectrum for CHA 0.2_15 after exposure to the $NO/O_2$ mixture at 200 °C (results from 3rd and final refinement step). The experimental data are shown as black open circles and the best fits with red solid lines. The scaled contributions stemming from each component ($Z[Cu^{II}NO_3]$ 8r and $Z_2Cu^{II}$ 6r models) are reported together with the optimized Cu-$Cu_{ef}$ SS path as coloured solid lines, vertically translated for sake of clarity.

## 3 WTA

### *3.1 Differential WT maps of the Cu-CHA samples pretreated in $O_2$ and exposed to the $NO/O_2$ mixture*

The differential WT maps, showed in **Figure S4** have been evaluated as the difference between the WT moduli of the samples exposed to the $NO/O_2$ mixture and the ones referring to the $O_2$ pretreatment.

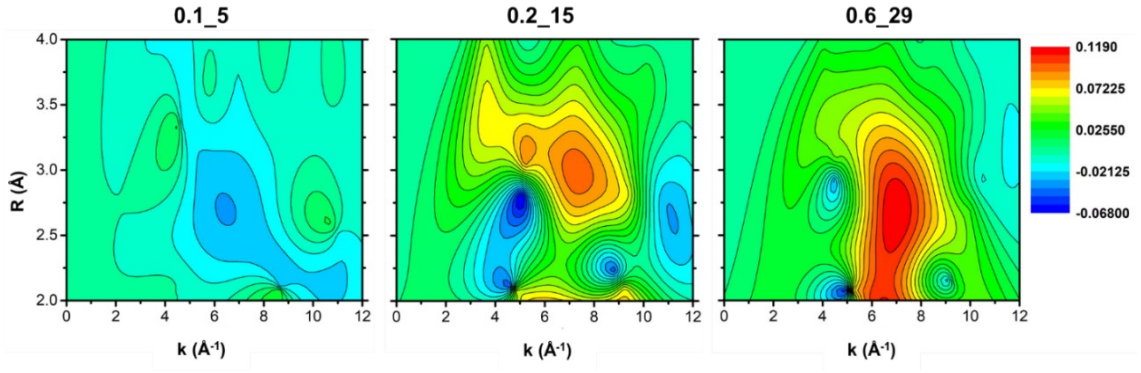


**Figure S4:** Differential WT representation of the EXAFS spectra associated to the Cu-CHA 0.1_5, Cu-CHA 0.2_15 and Cu-CHA 0.6_29 samples. The maps have been evaluated as the difference between the state pretreated in $O_2$ and the state exposed to the $NO/O_2$ mixture for each sample. The WT resolution parameters $\sigma$ and $\eta$ have been set to 1 and 7, respectively.

### *3.2 WTA of the best-fit EXAFS spectra for Cu-CHA 0.6_29 and Cu-CHA 0.1_15 after pretreatment*

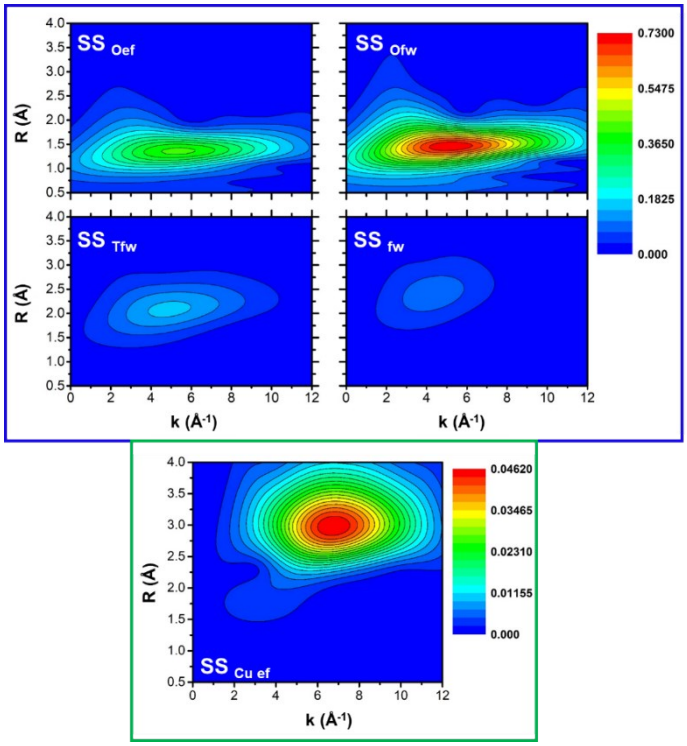


**Figure S5:** (a) WT representation of the individual EXAFS contributions, obtained from the best-fit results reported in **Table 2** of the main text for the Cu-CHA 0.6_29 sample pretreated in $O_2$. The labels associated to each map follow the ones adopted in **Figure 6**(b,c). The WT contribution proper of the Cu-$Cu_{ef}$ SS interaction has been plotted with a lower intensity scale in order to enhance its WT features and its

localization in both the k and R spaces. The WT resolution parameters $\sigma$ and $\eta$ have been set to 1 and 7, respectively.

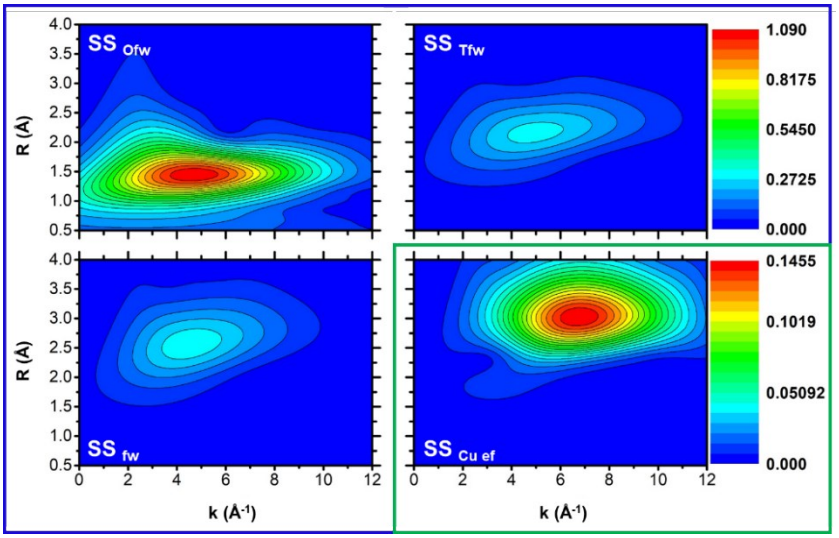


**Figure S6:** (a) WT representation of the individual EXAFS contributions, obtained from the best-fit results reported in **Table 2** of the main text for the Cu-CHA 0.1_5 sample pretreated in $O_2$. The labels associated to each map follow the ones adopted in **Figure 6**(e,f). The WT contribution proper of the Cu-$Cu_{ef}$ SS interaction has been plotted with a lower intensity scale in order to enhance its WT features and its localization in both the k and R spaces. The WT resolution parameters $\sigma$ and $\eta$ have been set to 1 and 7, respectively.

### *3.3 WTA of the best-fit EXAFS spectra for Cu-CHA 0.6_29 exposed to the NO/$O_2$ mixture*

Being in possess of a reliable model from EXAFS fitting, as reported in **Table 4** of the main text, it is possible to obtain a quantitative localization in the WT space of the SS and MS contributions shaping the experimental EXAFS spectrum. This approach is intriguing because it allows to explain the nature of the intense second lobe visible in the WT of the Cu-CHA 0.6_29 sample depicted in **Figure 5**, while leading to methodological considerations of general relevance in the context of WT EXAFS analysis. Focusing on the main paths composing EXAFS best-fit curve in **Figure 8(**b, c), it is possible to extract those paths specifically contributing to the second and third peaks observed the total EXAFS signal and to visualize them through the WT. The result of this procedure is reported in **Figure S7**. Herein, it is possible to note that the features occurring at low k-values are well described by scattering contributions involving the N atom of the $NO_3$ group and framework $T_{fw}$ atoms, extending in a larger region of the k-space. The reason of this behavior is not specific of this path but must identified as a broadening phenomenon, typical of the WT representation, that tends to distort in the k-space the WT features for low R-values, as discussed by Timoshenko and Kuzmin.[2] At higher R-values it is possible also to note the contribution deriving from farer framework atoms, principally O, and a minor contribution deriving from Si atoms indicated in the fit and in the WT plot as framework (fw) contribution.

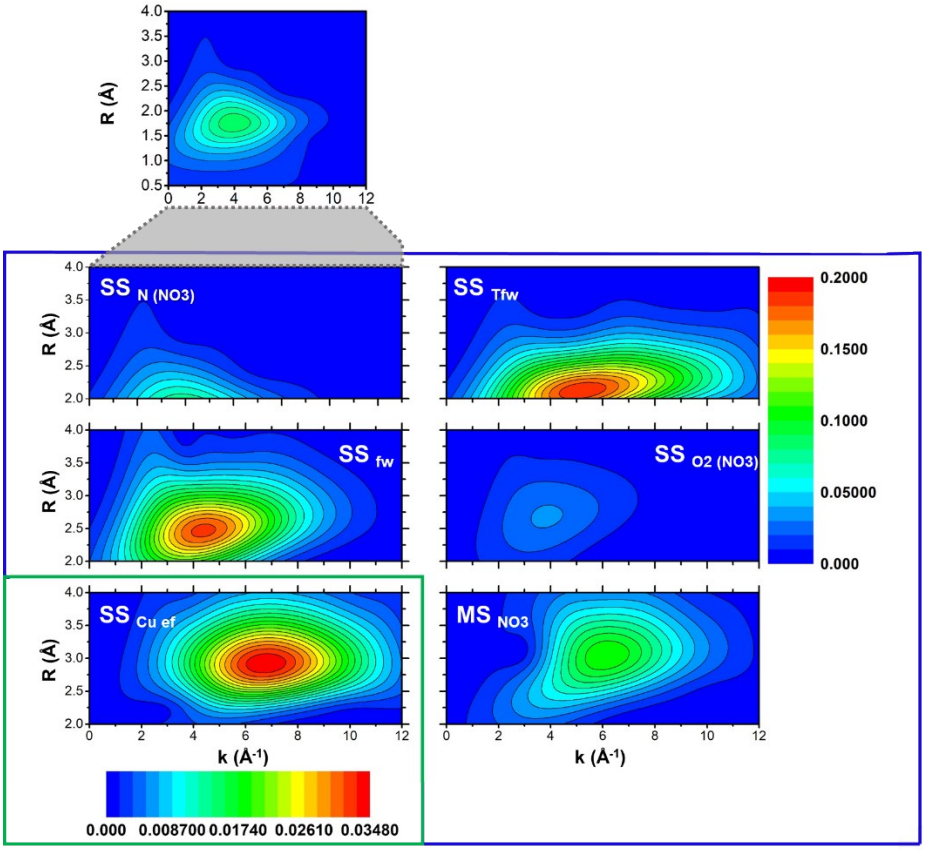


**Figure S7:** (a) WT representation of the individual EXAFS contributions, obtained from the best-fit results reported in **Table 4** of the main text for the Cu-CHA 0.6_29 sample exposed to the $NO/O_2$ mixture. The labels associated to each map follow the ones adopted in **Figure 8**(b,c). The upper inset shows the full R-range WT of the $N(NO_3)$ SS contribution, since the related WT representation is localized prevalently in the low R-values region. The WT contribution proper of the $Cu\text{-}Cu_{ef}$ SS interaction has been plotted with a lower intensity scale in order to enhance its WT features and its localization in both the k and R spaces. The WT resolution parameters $\sigma$ and $\eta$ have been set to 1 and 7, respectively.

The SS scattering contribution deriving from the O atom of the $NO_3$ group at higher R values ($SS\ O2_{NO3}$) is completely distinguishable from the $Cu\text{-}Cu_{ef}$ scattering path, which possess a $F(k)$ curve with a maximum located at ca 7.5 $Å^{-1}$, see **Figure S7** and **Figure S8**(a). Unfortunately, as indicated in section 3.2.3.1 of the main text, the $Cu\text{-}Cu_{ef}$ signal appears to be embedded inside the profile deriving from high-amplitude MS paths involving the atoms composing the $NO_3$ group and the oxygens framework in collinear or quasi-collinear configurations. Notably, these paths are individually characterized by $F(k)$ functions close to the backscattering amplitude trend proper of the O and N SS paths, see **Figure S8**(a,b), with a low k-value localization. However, in this range, the presence of certain MS signals in almost perfect antiphase determines the selective abatement of the total MS signal. The latter, in turn, is enhanced at high k-values where the all the MS signals return approximatively in phase, as showed in **Figure S8**(b). For sake of comprehension, the two most intense MS path signals in antiphase, composing part of the total MS contribution, are also presented in **Figure S8**(b), as grey and dark red signals. **Figure S8**(c) reports the two related scattering geometries responsible of these representative MS paths, using the same colour code. As a result, the total MS contribution in **Figure S8**(b) (i.e., the bottom violet signal), shows an *apparent* envelope extending within 4 and 10 $Å^{-1}$, centered at ca. 6.5 $Å^{-1}$ and largely overlapping in k-space with the weaker $Cu\text{-}Cu_{ef}$ signal. These considerations allow us to interpret the intense high-k feature observed in the experimental EXAFS WT plot for the Cu-CHA 0.6_29 sample upon exposure to the $NO/O_2$ mixture (**Figure 5** of the main text), and to properly reproduce its morphology based on EXAFS fitting results, as shown in **Figure S8**(d). Methodologically speaking, these results evidence how in the presence of unusually intense MS

contributions, as observed here, stemming from the combination of various scattering configurations packed in a tight R-space window, care should be taken in the visual interpretation of EXAFS WT maps. Structural analysis appears to be ultimately strengthened by combining conventional EXAFS fitting in R-space and WT visualization of individual scattering paths.

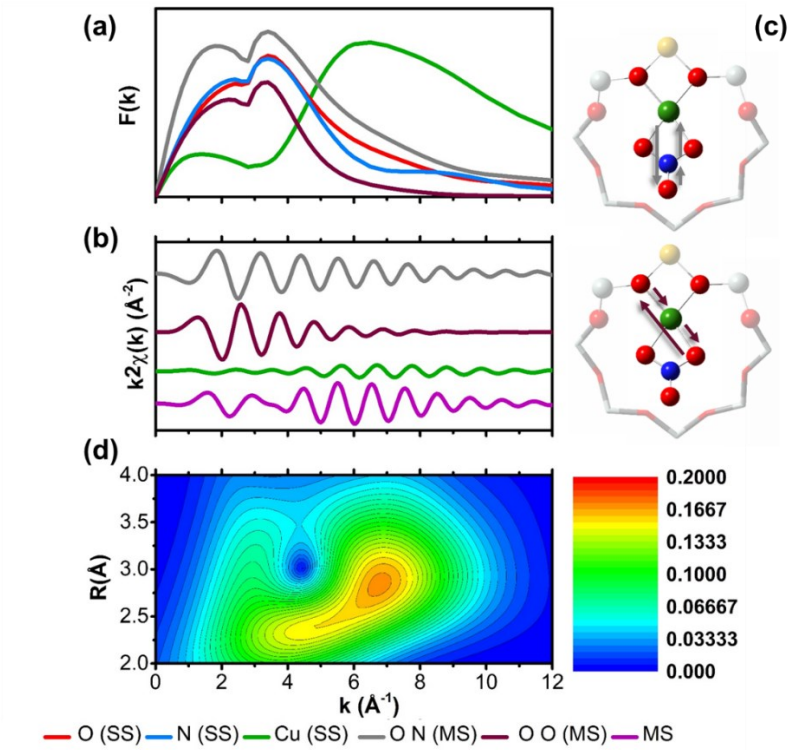


**Figure S8:** (a, b) Plot of the most intense MS $k^2\chi(k)$ contributions (in almost perfect antiphase) affecting the total MS signal reported at the bottom of the plot. For the sake of comparison, the Cu-$Cu_{ef}$ SS $k^2$-weighted signal is reported as well. (c) MS path geometries originating the Cu-ON and Cu-O-O MS signals reported in panel (b). (d) Total WT representation of the high-R EXAFS signal deriving from the fit reported in **Figure 8** of the main text. The WT resolution parameters $\sigma$ and $\eta$ have been set to 1 and 7, respectively.


1. C. Negri, P. S. Hammershøi, T. V. W. Janssens, P. Beato, G. Berlier and S. Bordiga, *Chemistry – A European Journal*, 2018, **24**, 12044-12053.
2. J. Timoshenko and A. Kuzmin, *Computer Physics Communications*, 2009, **180**, 920-925.